

## Supporting Information

### The role of Se vacancy and Fe doping on Nickel Selenide for Water Oxidation Reaction

Bishnupad Mohanty<sup>a,b</sup>, Bikash Kumar Jena<sup>b,c</sup>, Manikandan Kandasamy<sup>d</sup>, Namita Dalai<sup>a</sup>, Ranjan Kumar Sahu<sup>e</sup>, R.M. Kadam<sup>f</sup>, Bramhananda Chakraborty<sup>g,h\*</sup>, Bijayalaxmi Jena<sup>a\*</sup>

---

<sup>a</sup> Department of Chemistry, Utkal University, Bhubaneswar-751004, Odisha, India

<sup>b</sup> CSIR-Institute of Minerals and Materials Technology, Bhubaneswar-751013, India.

<sup>c</sup> Academy of Scientific & Innovative Research (AcSIR), Ghaziabad- 201002, India.

<sup>d</sup> Nonlinear Optical Materials Laboratory, School of Physics, Bharathidasan University, Tiruchirappalli-620024, Tamil Nadu, India.

<sup>e</sup> CSIR- National Metallurgical Laboratory, Jamshedpur-831007, India.

<sup>f</sup> Radio Chemistry Division, Bhabha Atomic Research Centre, Mumbai- 400085, India.

<sup>g</sup> High Pressure and Synchrotron Radiation Physics Division, Bhabha Atomic Research Centre, Mumbai- 400085, India.

<sup>h</sup> Homi Bhabha National Institute, Mumbai-400094, India.

## **Experimental section**

### **Materials**

Nickel (II) nitrate hexahydrate ( $\text{Ni}(\text{NO}_3)_2 \cdot 6\text{H}_2\text{O}$ , >98%), Iron (II) sulphate heptahydrate ( $\text{FeSO}_4 \cdot 7\text{H}_2\text{O}$ , >98.5%), Ammonium fluoride ( $\text{NH}_4\text{F}$ , >96%), Urea ( $\text{CH}_4\text{N}_2\text{O}$ , >99%), were purchased from HIMEDIA Chemical Reagent Co., Ltd, Sodium tetrahydroborate (>90%), Selenium powder (>99%) were purchased from Alfa Aesar Chemical Reagent Co., Ltd, Potassium hexachloro iridate (IV) [ $\text{K}_2\text{IrCl}_6$ ], Sodium citrate dibasic sesquihydrate (assay:  $\geq 99.0\%$ ), 5 wt% Nafion solution were purchased from Sigma- Aldrich.

### **Synthesis of NiFe-based precursor**

0.70 mmol nickel nitrate hexahydrate [ $\text{Ni}(\text{NO}_3)_2 \cdot 6\text{H}_2\text{O}$ ], 0.30 mmol iron sulphate hept-hydrate [ $\text{FeSO}_4 \cdot 7\text{H}_2\text{O}$ ], 5 mmol of ammonium fluoride ( $\text{NH}_4\text{F}$ ), 15 mmol urea ( $\text{NH}_2\text{CONH}_2$ ) were dissolved in 30 ml Millipore water. The solution was sonicated for 30 min and vigorously stirred for another 30 min to get a clear solution. After stirring the solution was transferred into a 50 mL Teflon-lined stainless-steel auto calve and heated at 140 °C in an electric oven for 12h. The material was washed with Millipore water, ethanol for three times to remove the unreacted molecule and finally the sample are dried at 60 °C in vacuum oven.

### **Synthesis of $\text{Ni}_{0.70}\text{Fe}_{0.30}\text{Se}_2$**

To the synthesized NiFe-based precursor, 5 mmol of Se powder, 10 mmol of sodium hydroxide and 0.2 ml of hydrazine hydrate are added in 30 ml dimethylformamide (DMF) solution. The solution was sonicated for 30 min followed by vigorous stirring for another 30 min. Then the solution was transferred into a 50 mL Teflon-lined stainless-steel auto calve and heated at

180 °C in an electric oven for 12h. After cooling down to room temperature, the substrate was washed with Millipore water, ethanol and dried at 60 °C in vacuum oven.

### **Synthesis of NiSe<sub>2</sub>**

The synthesis of NiSe<sub>2</sub> is same as followed for Ni<sub>0.70</sub>Fe<sub>0.30</sub>Se<sub>2</sub>. In synthesis of NiSe<sub>2</sub>, 1 mmol Ni (NO<sub>3</sub>)<sub>2</sub>·6H<sub>2</sub>O was used without adding FeSO<sub>4</sub>·7H<sub>2</sub>O.

### **Synthesis of V<sub>Se</sub>-Ni<sub>0.70</sub>Fe<sub>0.30</sub>Se<sub>2</sub>**

20 mg of synthesised Ni<sub>0.70</sub>Fe<sub>0.30</sub>Se<sub>2</sub> are dispersed in 10 ml of Millipore water and sonicated for 15 min. Then 0.095 g of NaBH<sub>4</sub> is added into it and stirred for different time (15, 30, 45 min). Then the solution was centrifuged three times with water and ethanol at 8000 rpm for 15 min each and dried in a vacuum oven for 12 hours at 60 °C.

### **Synthesis of IrO<sub>2</sub>/C**

The synthesis IrO<sub>2</sub>/C was carried out by previous reported method.<sup>1,2</sup> 100 mg of potassium hexachloroirridate (K<sub>2</sub>IrCl<sub>6</sub>) was added to 50 ml aqueous solution of 6.3×10<sup>-4</sup> M sodium hydrogen citrate sesquihydrate. The pH of the solutions was repeatedly adjusted to 7.5 by adding 0.25 M NaOH solutions and heated at 95 °C. The process was repeated until the pH was stabilized to 7.5. After that 0.184 g of carbon nano-powder was added to the above solutions and ultrasonicated for one hour. The solution was further heated at 95 °C for 2 hours by passing O<sub>2</sub> gas. The black precipitate was washed with water and ethanol three times. The sample was dried at 70 °C in vacuum pump for 12 hours. To remove the organic contaminant, the dried sample was heated at 300 °C for 30 minutes.

## Characterizations

PXRD patterns were recorded on X'pert PRO (Pan Analytical) X-ray diffraction unit using Ni filtered Cu K $\alpha$  ( $\lambda = 1.54 \text{ \AA}$ ) radiation at 40kV over a  $2\theta$  range of  $15^\circ$ - $80^\circ$ . Structural and morphological analysis of the as-synthesized samples were carried out by using field emission gun-based scanning electron microscope (FEG-SEM, Neon-40, Carl Zeiss) with 20 keV electrons. Transmission electron microscope (TEM) images were obtained using FEI-TECNAI G2 20S TWIN electron microscope 200 kV. The TEM grids were prepared by dissolving the sample in ethanol which was sonicated up to 1 hour and drop casted on carbon coated copper grids and were dried under the IR-Lamp of 100W lamp ( $\lambda > 400\text{nm}$ ) prior to analysis. X-ray photoelectron spectral (XPS) measurement was carried out using VG Scienta hemispherical analyser with resolution of 44.1 meV (Prevac, SI. No. 10001, Poland) well equipped with an Al-K $\alpha$  monochromatic source ( $\lambda = 1486.6 \text{ eV}$ ). The high-resolution spectra were deconvoluted using the Gaussian function. EPR spectrum of all sample recorded at X band frequency (9.5 GHz) at room temperature using Bruker (EMM1843) spectrometer.

## Electrochemical Measurements

The electrochemical measurements were carried by using the electrochemical work station in a two compartment three electrode electrochemical cell. High-purity KOH (99.98%) was used to prepare the 1M electrolyte. A platinum wire, Ag/AgCl and as synthesized material modified on glassy carbon electrodes (GCE,  $\sim 0.071 \text{ cm}^2$ ) are used as the counter, reference and working electrode respectively. Prior to the measurement, the GCE was mirror polished with slurry of alumina powder on a polishing pad, washed with deionised water followed by sonication and dried in vacuum desiccator. A catalyst ink was prepared by taking 1 mg of material, 5  $\mu\text{l}$  Nafion (5%) and 95  $\mu\text{l}$  ethanol and sonicated for 30 min. Then 5  $\mu\text{l}$  ink was drop

casted on the GCE electrode with loading of 0.7 mg/cm<sup>2</sup> and dried in a vacuum desiccator. Before the LSV measurement, all the catalysts are electrochemically preconditioned to reach the stable state i.e. the potential cycling between 0 and 0.8V (vs. Ag/AgCl) at scan rate of 100 mVs<sup>-1</sup>. For linear sweep voltammetry all the polarization curves were recorded at a scan rate of 5 mV s<sup>-1</sup>. All the potentials were converted to reversible hydrogen electrode (RHE) potential scale by using the equation 1,

$$E_{RHE} = E_{(Ag/AgCl)} + 0.0591 \times pH + E^0_{(Ag/AgCl)} \dots \dots \dots (1)$$

Here the value of E<sup>0</sup><sub>(Ag/AgCl)</sub> is 0.209 and the process takes places in 1 M KOH (pH=14) electrolyte for OER. The charge transfer efficiency of the electrocatalyst are studied by impedance spectroscopy at an overpotential of 300 mV by applying an AC voltage of 10 mV amplitude in a frequency range of 10000 Hz to 1 Hz. All Nyquist plots were fitted with the equivalent circuit. All the potentials presented here were iR-corrected, where “i” is the current and “R” is the uncompensated ohmic resistance of electrolyte solution which is determined from the Nyquist analysis. The Tafel slope is obtained by fitting the linear portions of the Tafel plots to the Tafel equation 2,

$$\eta = a + b \log j \dots \dots \dots (2)$$

where η is the overpotential, j is the current density and b is the Tafel slope. For OER, the over potential (η) was calculated by subtracting 1.23 V from the experimental potentials using the following equation 3,

$$\eta = E \text{ (vs. RHE)} - 1.23 \dots \dots \dots (3)$$

**Electrical Double Layered Capacitance measurement**

The electrochemical accessible surface area (ECSA) for all the electrocatalysts were derived from the double layered capacitance (Cdl) values. The catalysts were modified on the glassy carbon electrode (GCE). The CV were recorded in the non-Faradic region (0 to 0.1 V vs. Ag/AgCl) with scan rates of 20, 40, 80,120, 160 and 200 mV/s in 1M KOH electrolyte. To estimate Cdl, the plot between scan rate and the difference in current density variation ( $\Delta J = J_a - J_c$ ) at a particular overpotential are linearly fitted and the slope is twice the Cdl value. The current is directly proportional to the scan rates as per the following equation 4.

$$i = v C_{dl} \dots\dots\dots (4)$$

Then, the ECSA has been calculated by following the equation 5.

$$ECSA = C_{dl} / C_s \dots\dots\dots (5)$$

The  $C_s$  is the specific capacitance which is equal to  $0.04 \text{ mF cm}^{-2}$ . The roughness factor ( $R_f$ ) is calculated by dividing it by the geometrical surface area ( $0.071 \text{ cm}^2$ ).

The values of mass activity ( $\text{A g}^{-1}$ ) were calculated from the catalyst loading  $m$  ( $0.7 \text{ mg cm geo}^{-2}$ ) and the measured current density  $j$  ( $\text{mA cm geo}^{-2}$ ) at  $\eta = 280 \text{ mV}$

$$\text{Mass activity} = j/m \dots\dots\dots (6)$$

**Estimation of the number of active sites (n)**

The number of active sites and TOF are calculated by previous reported method.<sup>3</sup> First, to calculate the number of active sites (n), CV data are recorded in the potential range of -0.82V to -0.023 V vs Ag/AgCl in 1M phosphate buffer (pH=7) electrolyte with scan rate of 50 mV/s.

The value of n is calculated by using the equation 7

$$n = Q_{cv} / 2F \dots\dots\dots (7)$$

Where  $Q_{cv}$  is the integrated charge derived from CV and F is the Faraday constant .

### Estimation of turn over frequency (TOF)

The TOF value was derived using the equation 8.

$$TOF = I / 4 \times F \times n \dots \dots \dots (8)$$

where I is the current in ampere and F is Faraday constant.

### Mott-Schottky (M-S) Analysis

For M-S analysis, capacitance measurement takes place at 1 kHz frequency. The donor density ( $N_d$ ) and flat band potentials ( $V_{fb}$ ) were estimated by using the equations.<sup>4,5</sup>

$$\frac{1}{C^2} = \frac{2}{eA^2N_d\epsilon\epsilon_0} \left( V - V_{fb} - \frac{KT}{e} \right) \dots \dots \dots (9)$$

$$N_d = \frac{2}{e\epsilon\epsilon_0} \left[ \frac{dE}{d\left(\frac{1}{C^2}\right)} \right] \dots \dots \dots (10)$$

where C and A represent the interfacial capacitance and area respectively, V is the applied voltage, k is the Boltzmann's constant, T is the absolute temperature,  $e_0$  is the electron charge,  $\epsilon$  is the dielectric constant,  $\epsilon_0$  is the permittivity of vacuum. The flat band potential can be measured by extrapolation of liner fitted curve to the X-axis at a point  $1/C^2 = 0$ .

### Rotating disk electrode voltammetry

RRDE experiments were carried out using a VSP-300 multi-channel potentiostat (Biologic Inc), a rotator, GC Disk-Pt Ring of Pine instruments USA. The disk electrode was scanned at a rate of  $10 \text{ mV s}^{-1}$  and the ring electrode potential was set to 1.48 V versus RHE. The hydrogen peroxide yield ( $\text{H}_2\text{O}_2$  %), and Faradic efficiency (FE) were determined by the following equations<sup>6,7</sup>

$$\text{H}_2\text{O}_2(\%) = 100 \frac{2 \times \frac{I_r}{N}}{I_d + \frac{I_r}{N}} \dots \dots \dots (11)$$

$$FE = \frac{I_r}{N \times I_d} \dots \dots \dots (12)$$

where  $I_d$  is the disk current,  $I_r$  is the ring current and  $N = \sim 0.2$  is the current collection efficiency of the Pt ring.

### Computational Details

To provide theoretical support for the obtained experimental results, the first principles simulation has been done by the projector augmented wave (PAW) method as implemented in the VASP code.<sup>8-11</sup> Here, the respective PAW-GGA pseudo potential has been used for the Ni, Se and Fe atoms.<sup>12</sup> For the bulk NiSe<sub>2</sub>, we have used the Monkhorst Pack mesh of (9x9x9)  $k$ -points and for the surface 5x5x1  $k$ -points were taken. The convergence criteria for total energy and Hellmann-Feynman forces are taken as  $10^{-6}$  eV and 0.01 eV/Å respectively.



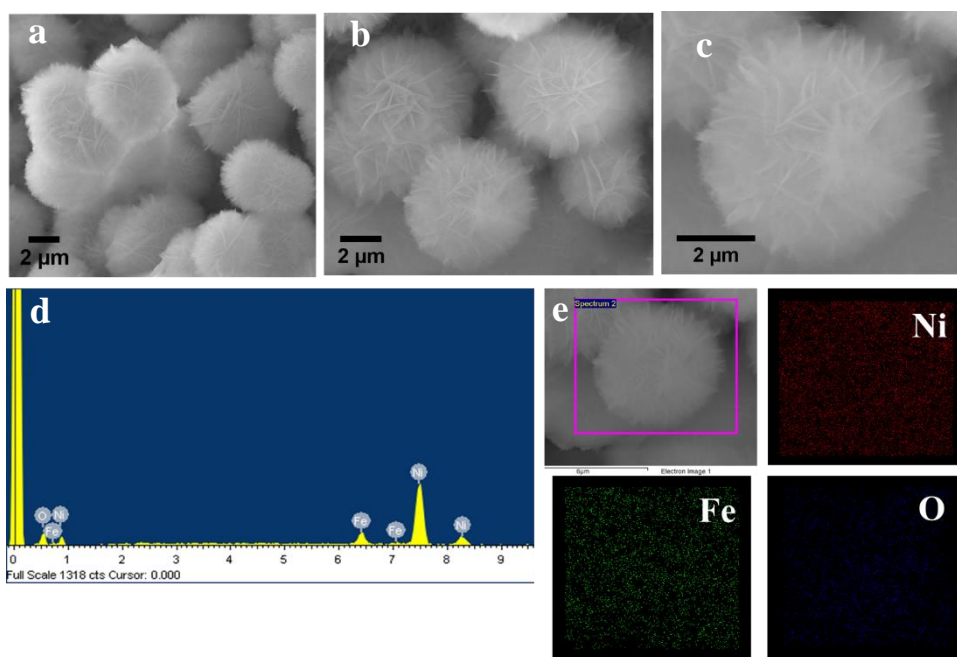


**Figure S1.** (a, b, c) FESEM image of NiFe-LDH (d) EDX Spectrum of NiFe-LDH (e) its Elemental colouring mapping.

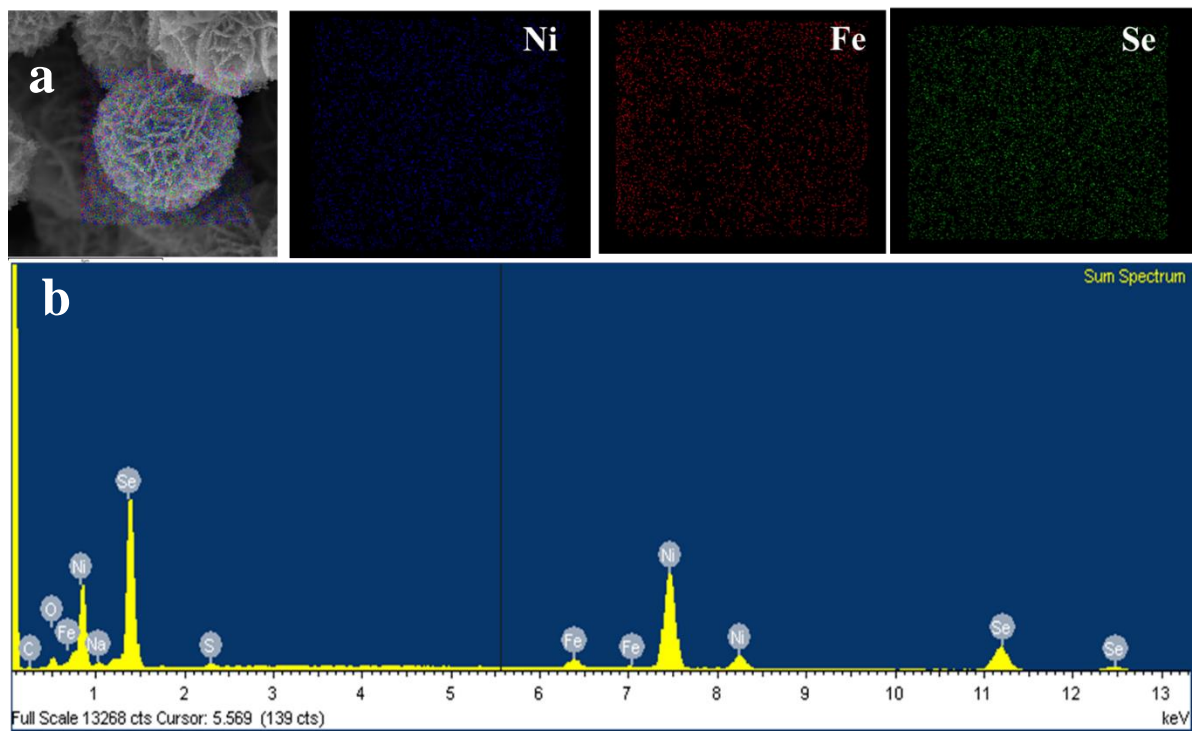


**Figure S2.** (a) Elemental colouring mapping (b) EDX Spectrum of  $\text{Ni}_{0.70}\text{Fe}_{0.30}\text{Se}_2$ .

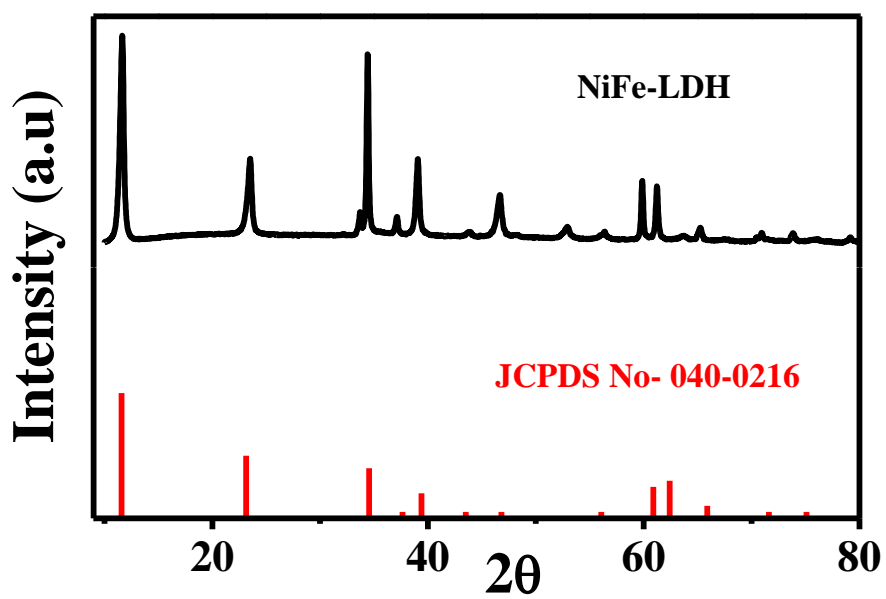


**Figure S3.** XRD pattern of NiFe-LDH.

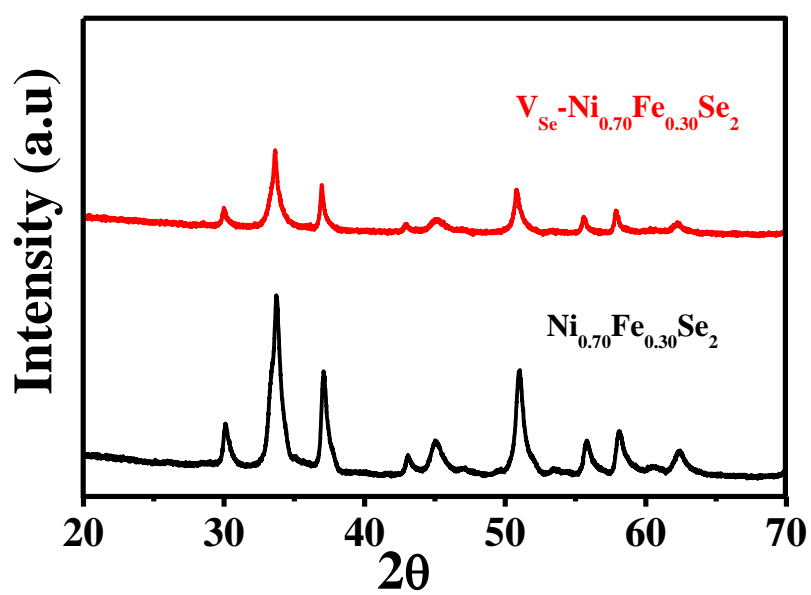


**Figure S4.** XRD patterns of  $Ni_{0.70}Fe_{0.30}Se_2$  before and after vacancies creation.

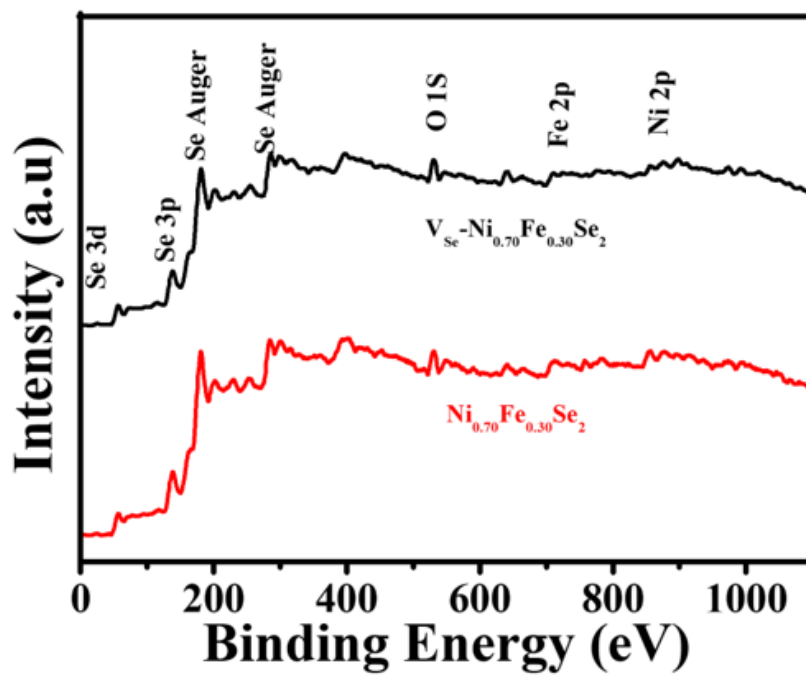


**Figure S5.** Full survey scan XPS spectra of  $Ni_{0.70}Fe_{0.30}Se_2$  and  $V_{Se}-Ni_{0.70}Fe_{0.30}Se_2$

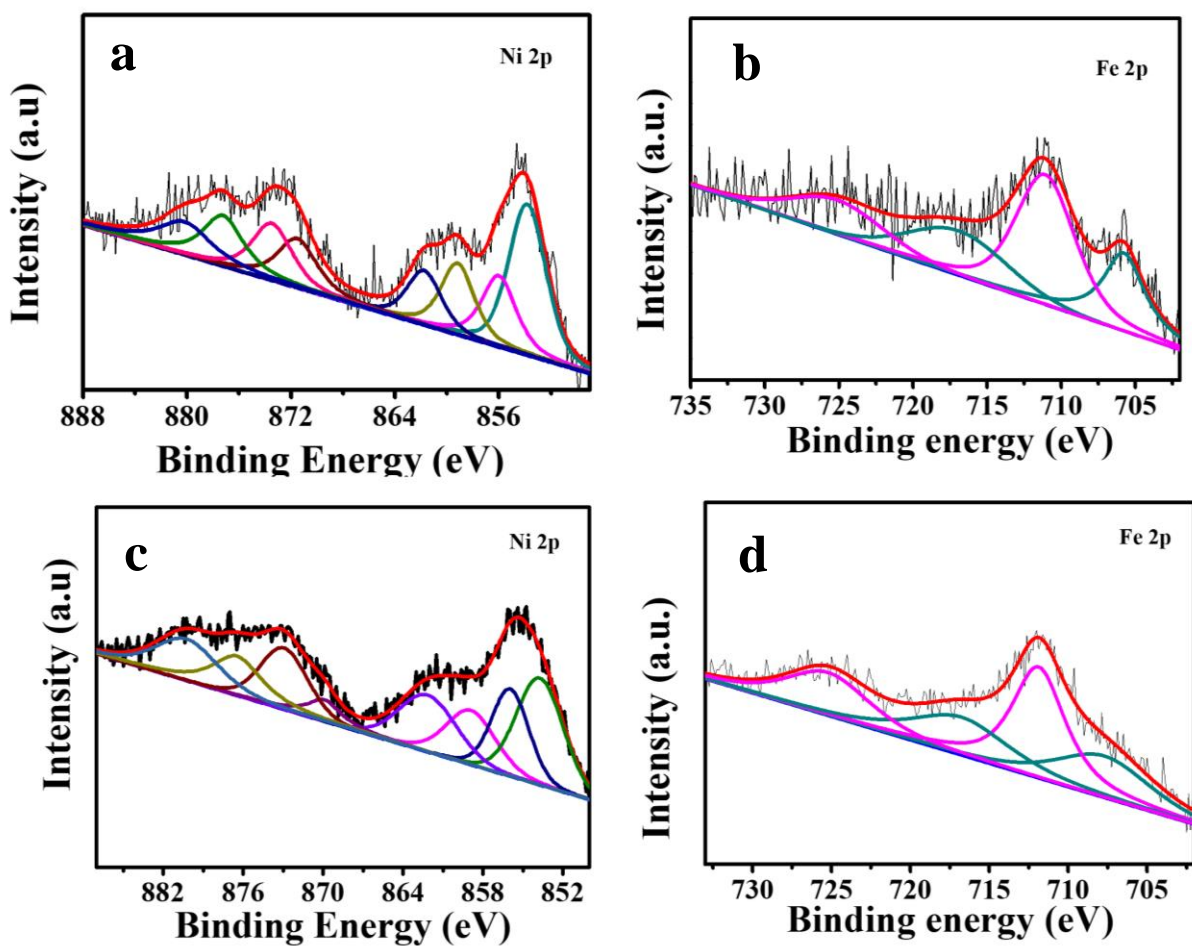


**Figure S6.** XPS spectra (a) Ni 2p; (b) Fe 2p for  $V_{Se}-Ni_{0.70}Fe_{0.30}Se_2$  nanoflowers and (c) Ni 2p; (d) Fe 2p for  $Ni_{0.70}Fe_{0.30}Se_2$ .

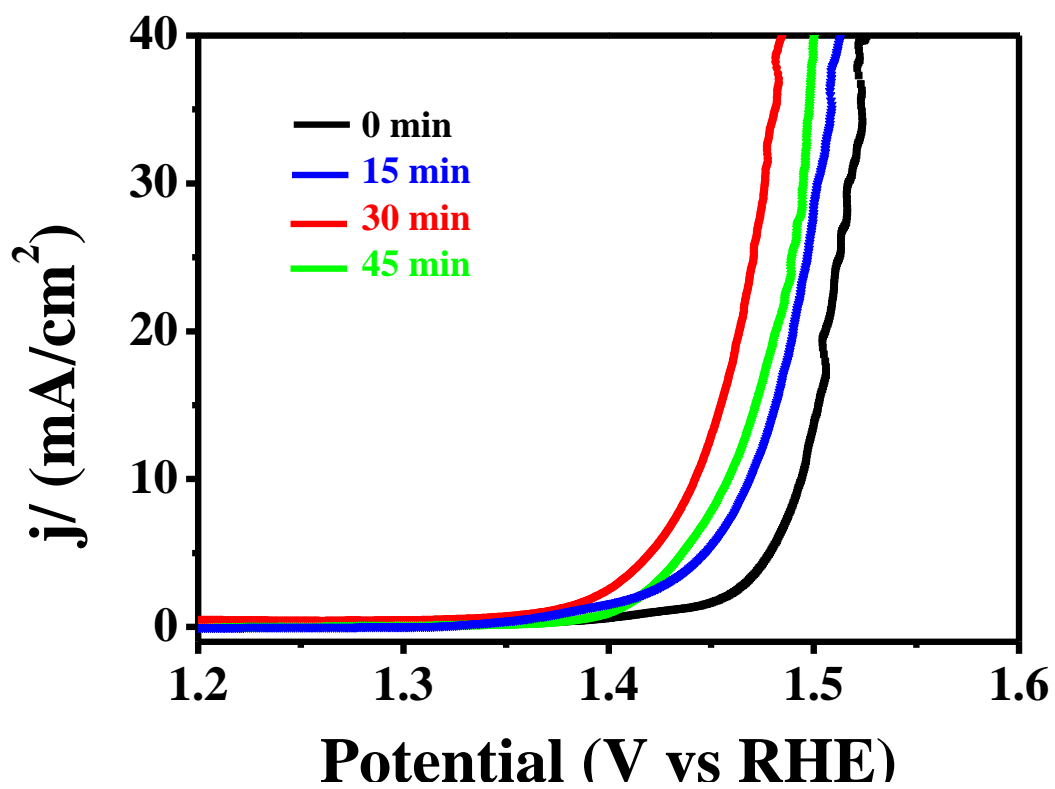
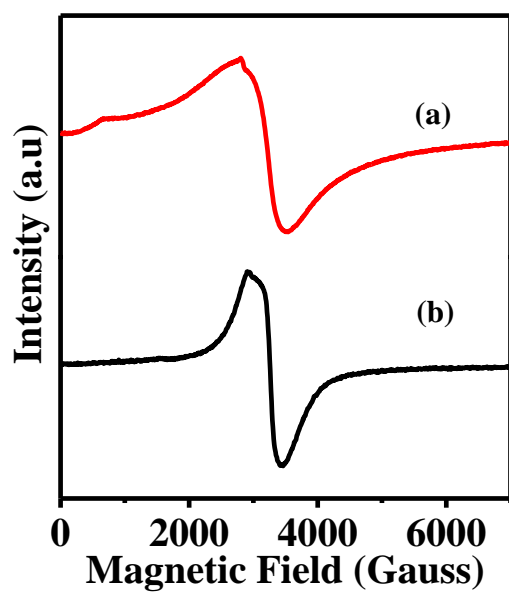
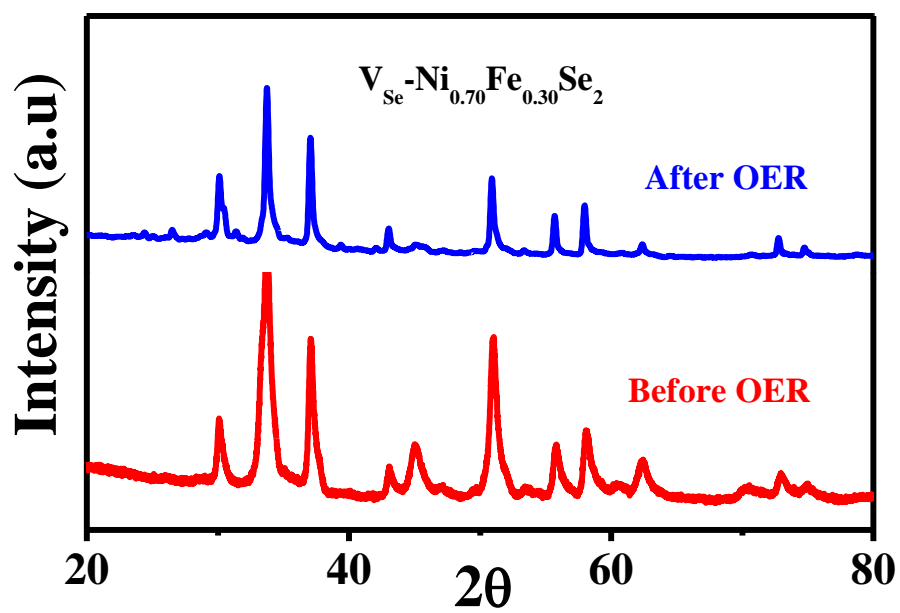


Figure S7. LSV curve of V<sub>Se</sub>-Ni<sub>0.70</sub>Fe<sub>0.30</sub>Se<sub>2</sub> with different reduction time.



**Figure S8.** EPR data of  $\text{VSe-Ni}_{0.70}\text{Fe}_{0.30}\text{Se}_2$  (a) before and (b) after OER.





**Figure S9.** PXRD data of  $V_{Se}-Ni_{0.70}Fe_{0.30}Se_2$  before and after LSV measurement.

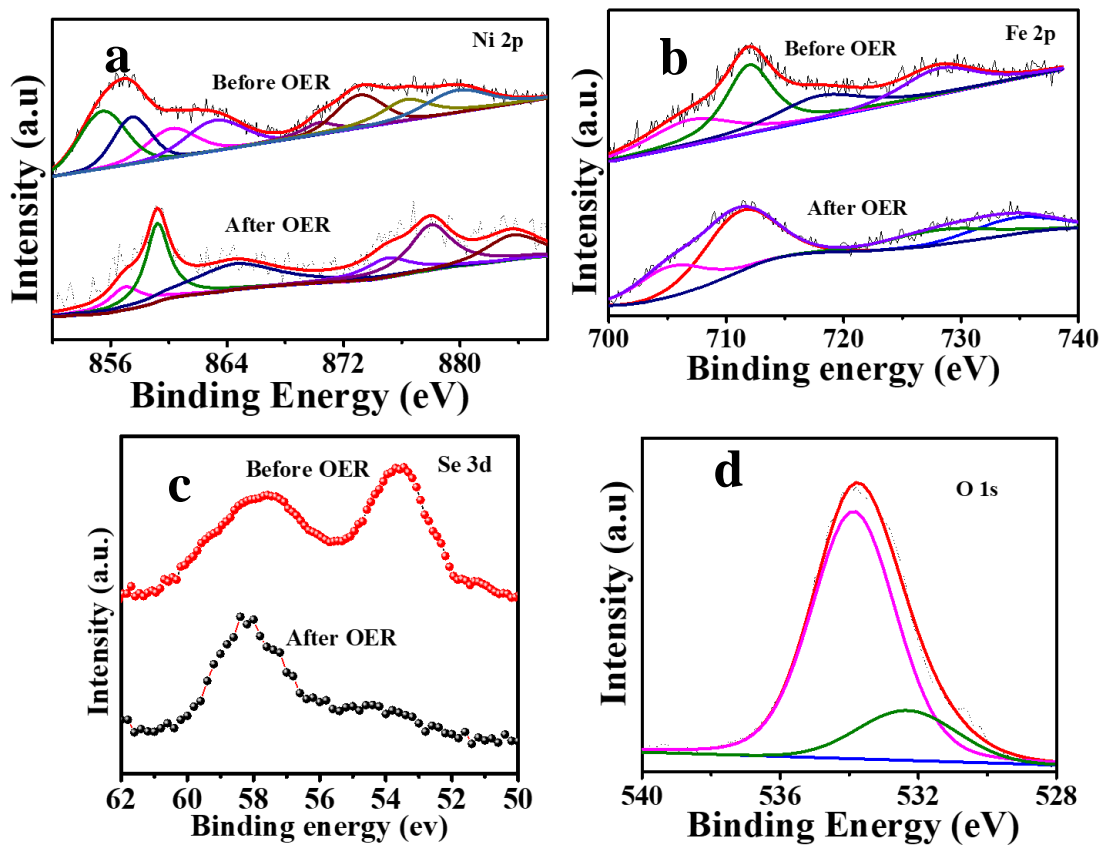


**Figure S10.** Before and after OER XPS spectra of  $V_{Se}-Ni_{0.70}Fe_{0.30}Se_2$  (a) Ni 2p (b) Fe 2p (c) Se 3d (d) O 1s.

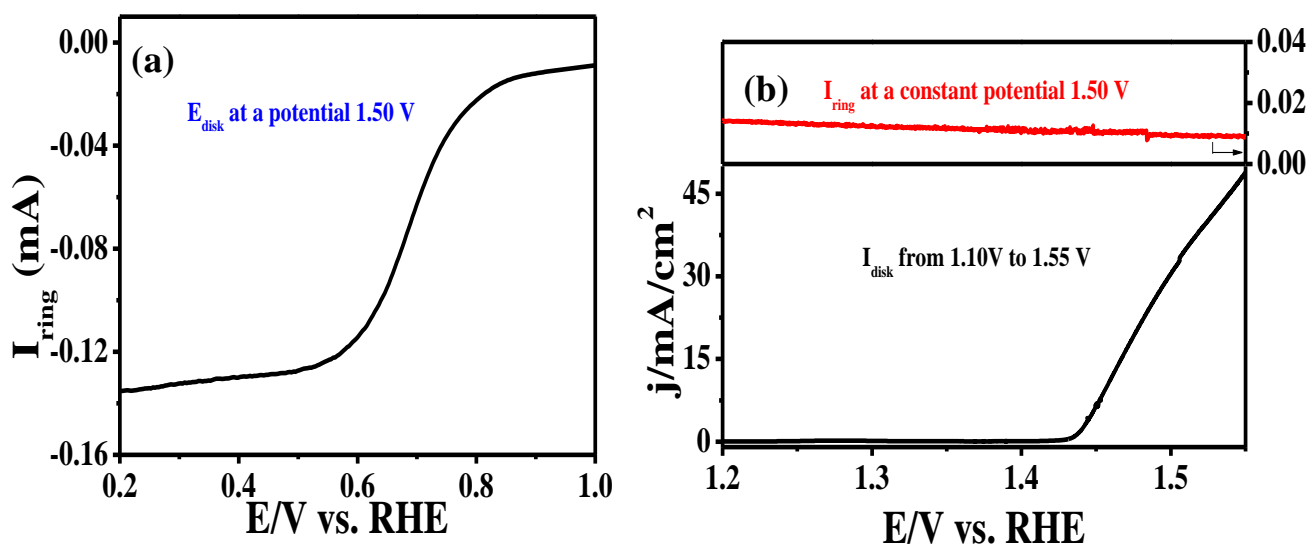


**Figure S11.** RRDE measurements to evaluate the oxygen formation and electron transfer number during OER of  $\text{VSe-Ni}_{0.70}\text{Fe}_{0.30}\text{Se}_2$ . (a) LSV curve of oxygen reduction reaction (ORR) at disk potential 1.50V in Ar-saturated 1M KOH solution. (b) RRDE measurement in  $\text{O}_2$ -saturated 1M KOH solution (ring potential: 1.50 V).

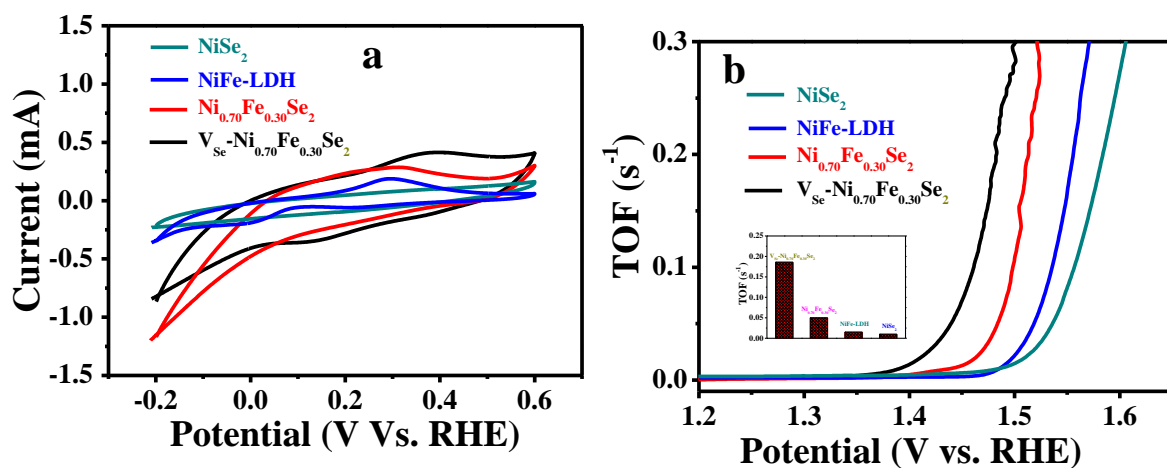


**Figure S12.** (a) CVs of as-synthesised materials in phosphate buffer (pH = 7) at a scan rate of 50 mV/s. (b) TOF plot of different as-synthesized catalysts towards OER, its inset shows the bar plot of TOF values of all the electrocatalysts at the overpotential of 250mV.

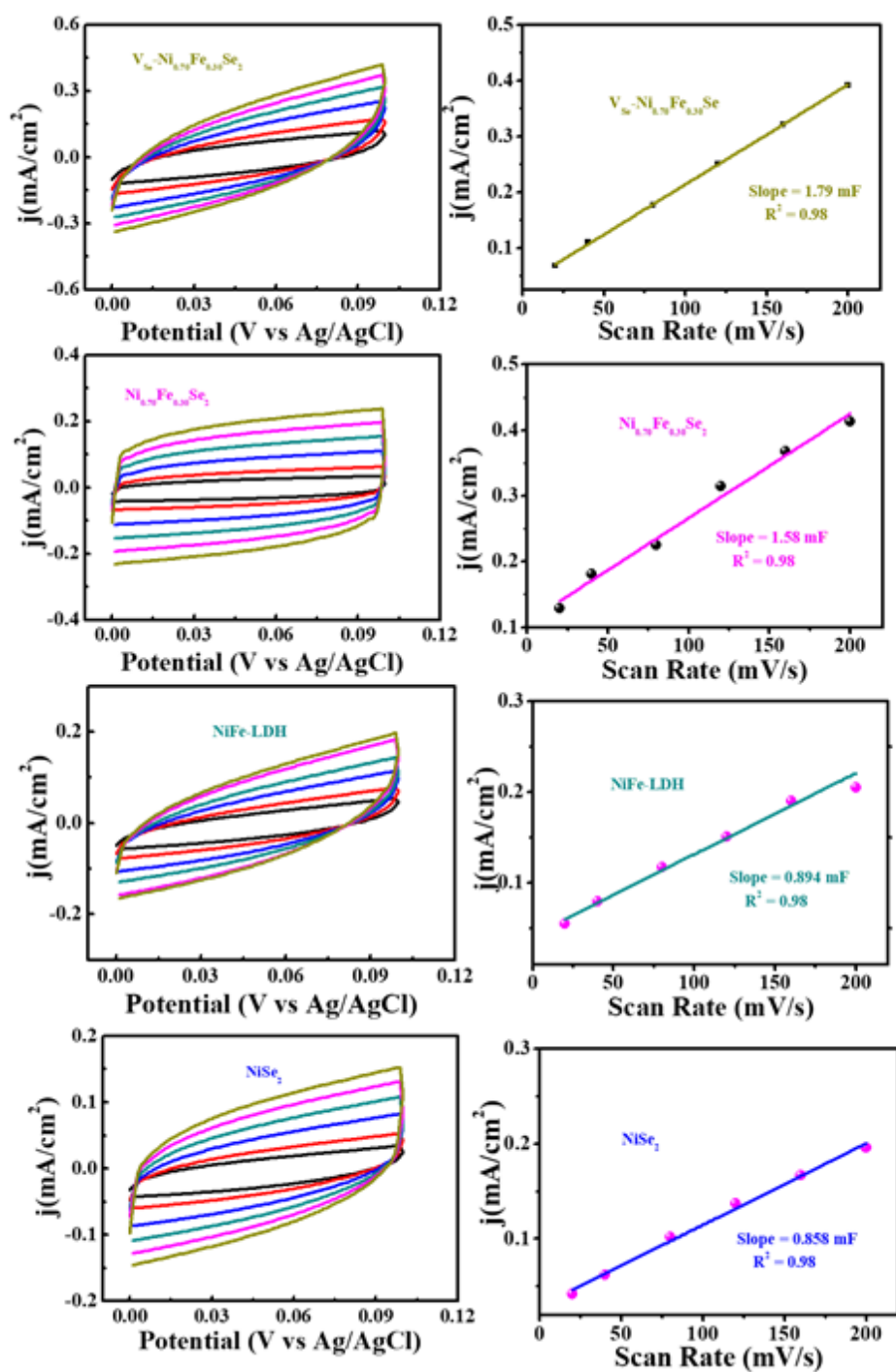


**Figure S13.** Cyclic voltammograms obtained from the non-Faradic region of as-synthesized  $V_{Se}-Ni_{0.70}Fe_{0.30}Se_2$ ,  $Ni_{0.70}Fe_{0.30}Se_2$ , NiFe-LDH,  $NiSe_2$  catalyst at different scan rates. The corresponding plot of scan rate vs the anodic current measured at 0.05V.

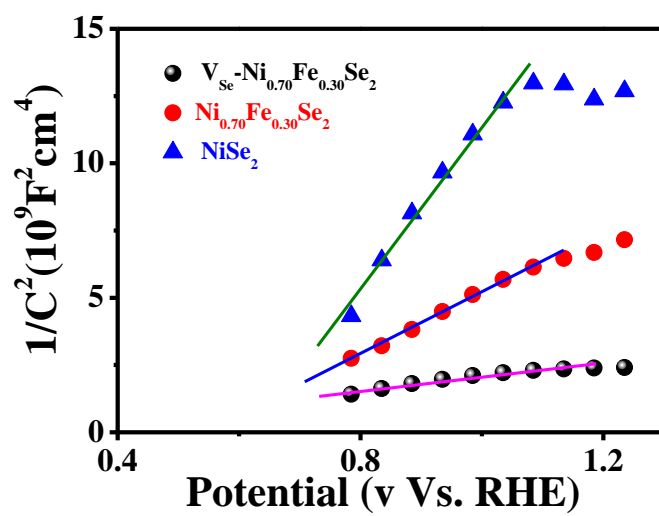
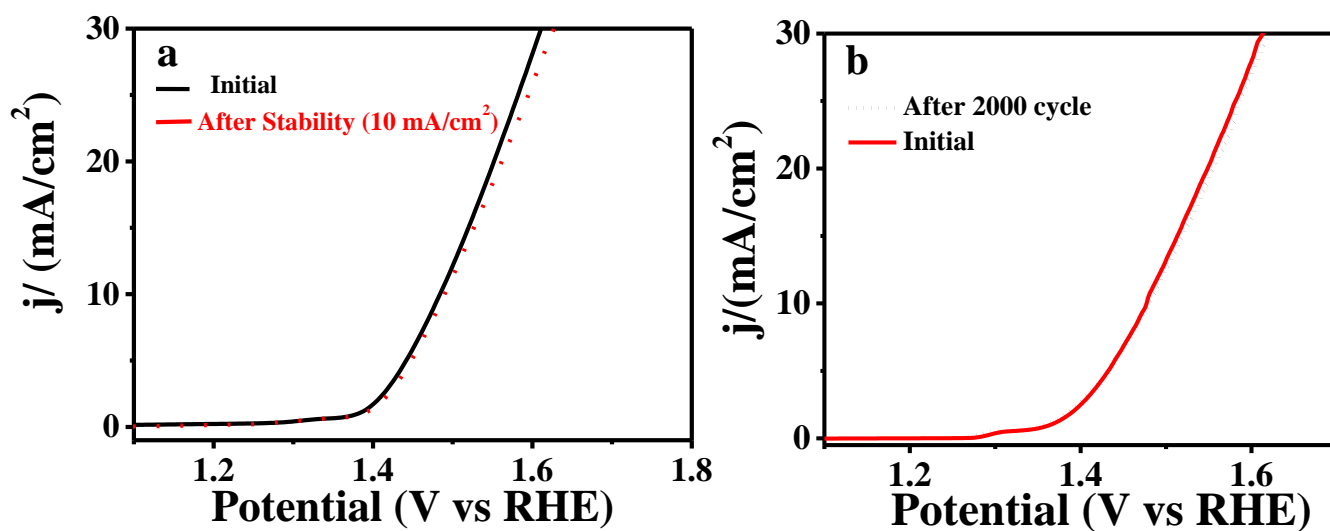
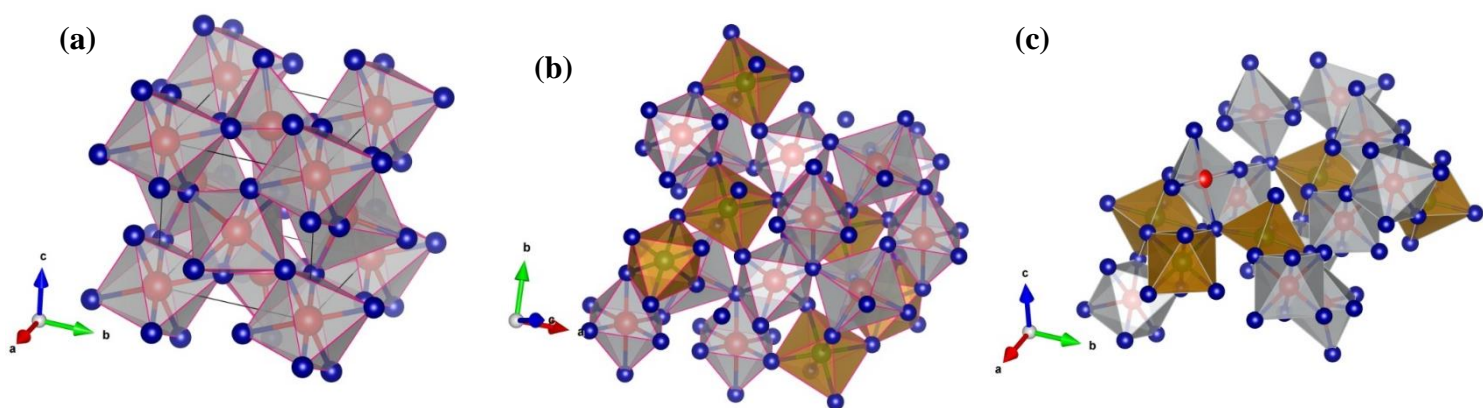


Figure S14. Mott Schottky plot for all the catalysts in 1M KOH.



**Figure S15.** (a) LSV curve of  $V_{Se}-Ni_{0.70}Fe_{0.30}Se_2$  before and after chronopotentiometric measurement. (b) LSV curve after cyclic stability.



**Figure S16.** DFT optimized bulk structure of (a)  $\text{NiSe}_2$  (b)  $\text{Ni}_{0.70}\text{Fe}_{0.30}\text{Se}_2$  (c)  $\text{VSe}-\text{Ni}_{0.70}\text{Fe}_{0.30}\text{Se}_2$ . Red, Blue and Green color represent Ni, Se and Fe atoms respectively.



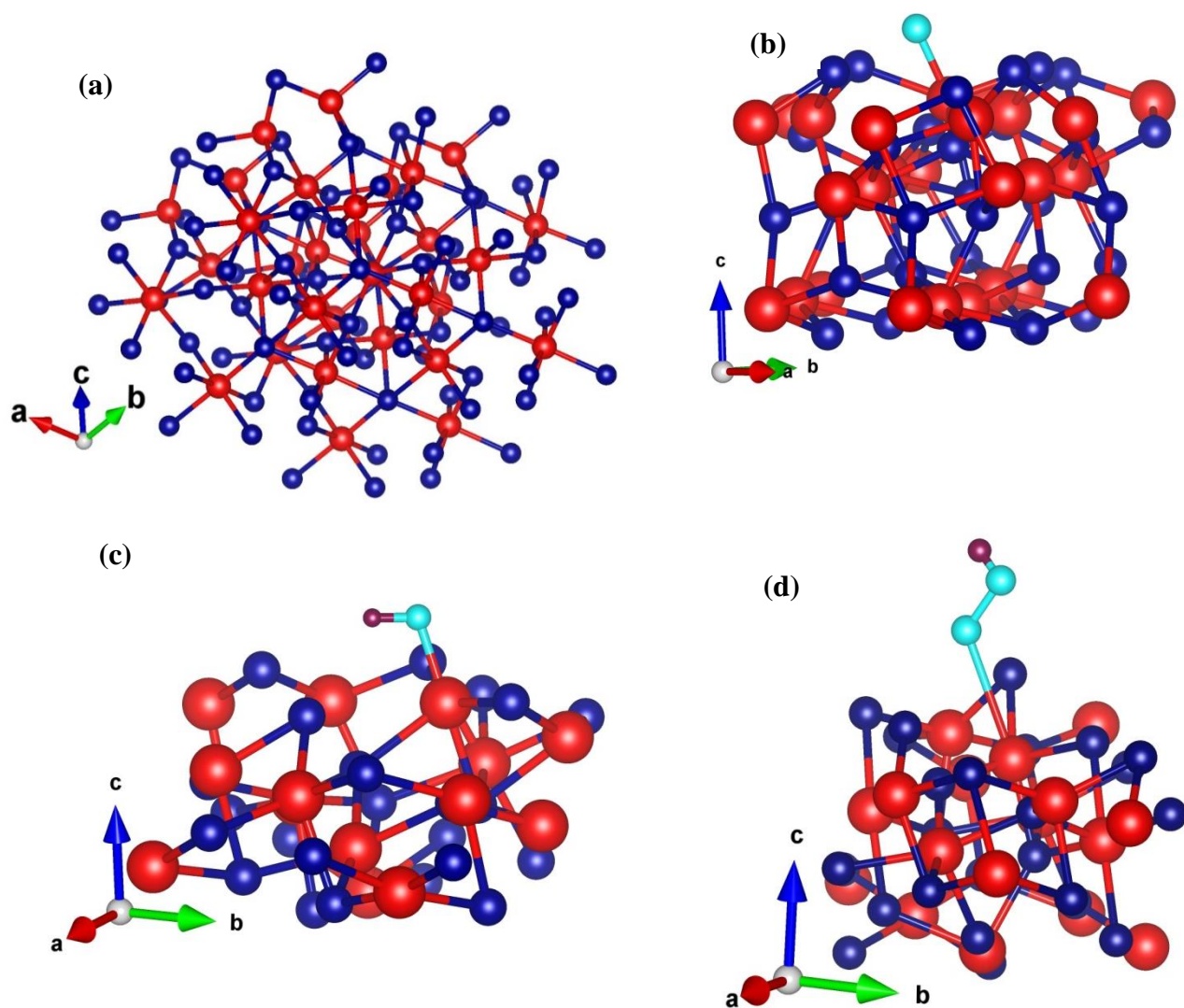


**Figure S17.** DFT optimized Structure of (a) NiSe<sub>2</sub> (200) surface, (b) adsorption configuration of O on NiSe<sub>2</sub> (200) surface (c) adsorption configuration of OH on NiSe<sub>2</sub> (200) surface and (d) adsorption configuration of OOH on NiSe<sub>2</sub> (200) surface. Red, Blue, Cyan, brown represents Ni, Se, O, H respectively.

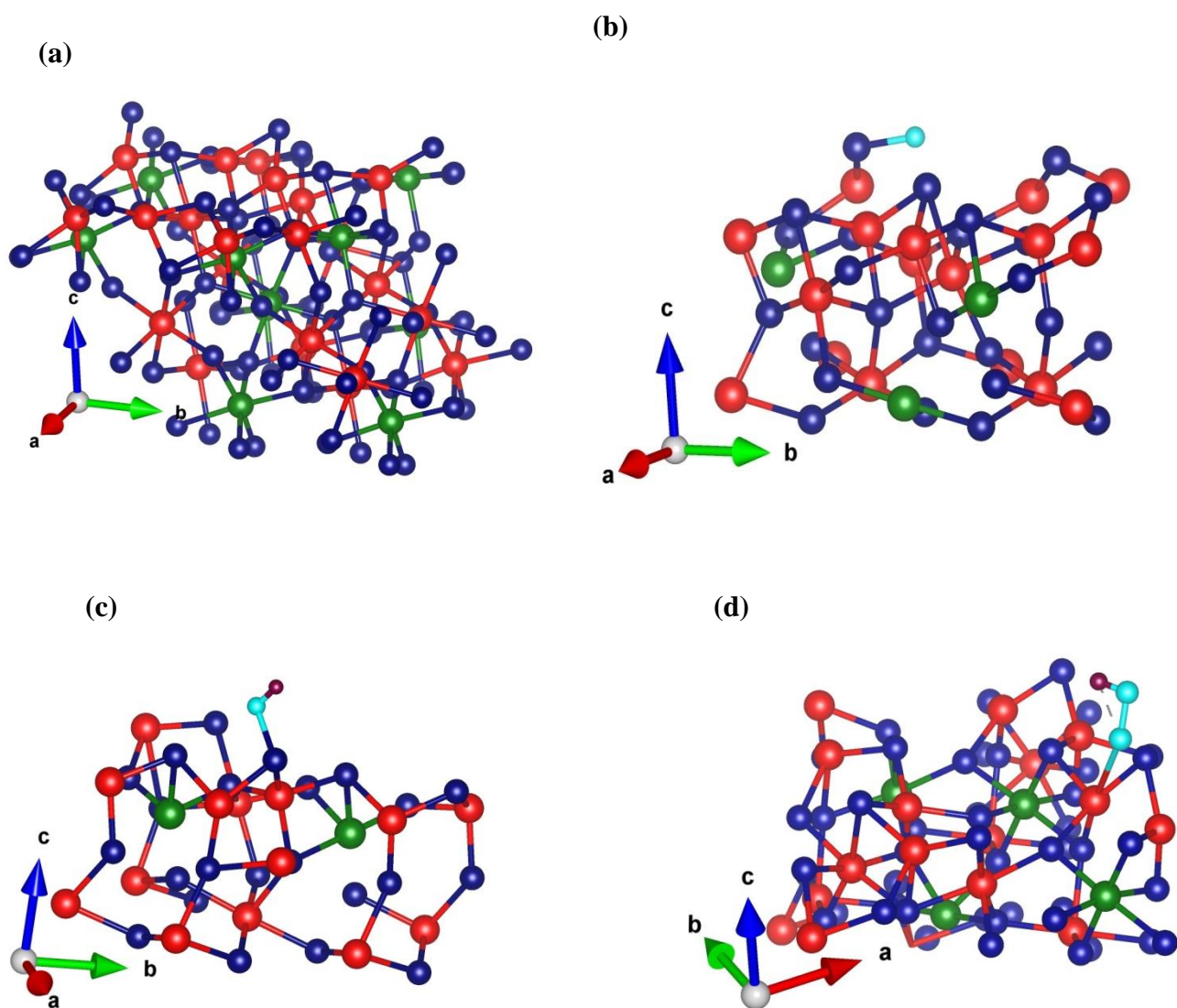


**Figure S18.** DFT optimized Structure of (a)  $\text{Ni}_{0.70}\text{Fe}_{0.30}\text{Se}_2$  (200) surface, (b) adsorption configuration of O on  $\text{Ni}_{0.70}\text{Fe}_{0.30}\text{Se}_2$  (200) surface (c) adsorption configuration of OH on  $\text{Ni}_{0.7}\text{Se}_2\text{Fe}_{0.3}$  (200) surface and (d) adsorption configuration of OOH on  $\text{Ni}_{0.7}\text{Se}_2\text{Fe}_{0.30}$  (200) surface. Red, Blue, Cyan, Brown represents Ni, Se, O and H respectively.

**Table S1: ICP results of Ni<sub>0.7</sub>Fe<sub>0.3</sub>Se<sub>2</sub> catalysts.**

Sample	Ni (wt. %)	Fe (wt. %)	Se (wt. %)	Elemental molar ratio
Ni <sub>0.7</sub> Fe <sub>0.3</sub> Se <sub>2</sub>	35	11	51	3.18:1:7.513

**Table S2: XPS data analysis in detail for Ni<sub>0.7</sub>Fe<sub>0.3</sub>Se<sub>2</sub>, V<sub>Se</sub>-Ni<sub>0.7</sub>Fe<sub>0.3</sub>Se<sub>2</sub> and V<sub>Se</sub>-Ni<sub>0.7</sub>Fe<sub>0.3</sub>Se<sub>2</sub>**

Catalysts	Ratio of Se/Ni (%)	Ratio of Se/Fe (%)	Ratio of Ni <sup>+2</sup> /Ni <sup>3+</sup>	Ratio of Fe <sup>+2</sup> /Fe <sup>3+</sup>
Ni <sub>0.7</sub> Fe <sub>0.3</sub> Se <sub>2</sub>	4.43	5.61	0.17	1.53
V <sub>Se</sub> -Ni <sub>0.7</sub> Fe <sub>0.3</sub> Se <sub>2</sub>	2.73	1.73	0.35	1.91
V <sub>Se</sub> -Ni <sub>0.7</sub> Fe <sub>0.3</sub> Se <sub>2</sub> After OER	2.48	1.56	0.21`	1.51

**Table S3: OER performance of our as-synthesised  $V_{Se}-Ni_{0.7}Fe_{0.3}Se_2$  with other catalysts.**

Catalysts	Electrolyte	$\eta_{10}$	Tafel (mV/dec)	Substrate	Reference
$Ni_{0.76}Fe_{0.24}Se$	1M KOH	197	56	Ni foam	Nano Research 2018, 11, 2149
Fe-NiSe	1M KOH	233	48	Ni foam	J. Mater. Chem. A, 2017, 5, 14639
$Ni_{0.5}Fe_{0.5}Se_2$	1M KOH	255	47.2	CFC	ACS Appl. Mater. Interfaces, 2016, 8, 19386
$Ni_xFe_{1-x}Se_2$ -DO	1M KOH	195	28	Ni foam	Nat. Commun. 2016,7, 12324
$Ni_{1.12}Fe_{0.49}Se_2$	1M KOH	227	37.9	XC-72	Nanoscale, 2017,9, 6821
$Ni_{0.75}Fe_{0.25}Se_2$	1M KOH	272	56	GCE	Electrochim. Acta. 2018, 286, 172
$Ni_3S_2/NF-4$	1M KOH	242	76	Ni foam	ACS Appl. Mater. Interfaces.2018,10, 37
$Ni_3Se_2$	1M KOH	315 ( $\eta^{100}$ )	40.2	Ni foam	Appl. Catal. B-Environ., 2017, 203, 485
Co-Ni-Se/C	1M KOH	300 ( $\eta^{50}$ )	63	Ni foam	J. Mater. Chem. A, 2016, 4, 15148
NiSe nanowires	1 M KOH	270 ( $\eta^{20}$ )	64	Ni foam	Angew. Chem. Int. Ed., 2015, 54, 9351
Fe-Ni-Se/NF	1 M KOH	290 ( $\eta^{60}$ )	61	Ni foam	Inorg. Chem. Front., 2018,5, 814
$Ni_3Se_2$ -Ni foam	1 M KOH	270	142	Ni foam	Energy Environ. Sci., 2016, 9, 1771
$Ni_3Se_4$	1 M KOH	244	30	Ni foam	ACS Appl. Mater. Interfaces. 2017, 9, 8714
$Co_{0.13}Ni_{0.87}Se_2/Ti$	1 M KOH	320 ( $\eta^{100}$ )		Ti	Nanoscale, 2016, 8, 3911
$V_{Se}-Ni_{0.7}Fe_{0.3}Se_2$	1M KOH	210	61	GCE	This work

**Table S4: Comparison of different electrochemical parameter of as synthesized catalysts**

<b>Catalysts</b>	<b>Cdl (mF/c m<sup>2</sup>)</b>	<b>ECSA</b>	<b>Rf</b>	<b>Mass Activity</b>	<b>TOF at <math>\eta=250</math> mV</b>	<b>R<sub>ct</sub> (<math>\Omega</math>)</b>	<b>Tafel Slope (mV/dec)</b>
<b>V<sub>Se</sub>-Ni<sub>0.70</sub>Fe<sub>0.30</sub>Se<sub>2</sub></b>	0.895	22.73	559.25	85.73	0.186	34.88	61
<b>Ni<sub>0.70</sub>Fe<sub>0.30</sub>Se<sub>2</sub></b>	0.79	19.75	278.16	31.55	0.050	65.80	68
<b>NiFe-LDH</b>	0.44	11	154.92	2.87	0.015	110.9	75
<b>NiSe<sub>2</sub></b>	0.42	10.5	147.88	1.57	0.010	171.2	82

## References:

- 1 B. Mohanty, M. Ghorbani-Asl, S. Kretschmer, A. Ghosh, P. Guha, S. K. Panda, B. K. B. Jena, A. V Krasheninnikov and B. K. B. Jena, *ACS Catalysis*, 2018, **0**, null.
- 2 P. Bhanja, B. Mohanty, A. K. Patra, S. Ghosh, B. K. Jena and A. Bhaumik, *ChemCatChem*, 2019, **11**, 583–592.
- 3 S. Kamila, B. Mohanty, A. K. Samantara, P. Guha, A. Ghosh, B. Jena, P. V Satyam, B. K. Mishra and B. K. Jena, *Scientific Reports*, 2017, **7**, 8378.
- 4 K. Gelderman, L. Lee and S. W. Donne, *Journal of Chemical Education*, 2007, **84**, 685.
- 5 S. Bolar, S. Shit, J. S. Kumar, N. C. Murmu, R. S. Ganesh, H. Inokawa and T. Kuila, *Applied Catalysis B: Environmental*, 2019, **254**, 432–442.
- 6 S. Zhao, Y. Wang, J. Dong, C.-T. He, H. Yin, P. An, K. Zhao, X. Zhang, C. Gao, L. Zhang, J. Lv, J. Wang, J. Zhang, A. M. Khattak, N. A. Khan, Z. Wei, J. Zhang, S. Liu, H. Zhao and Z. Tang, *Nature Energy*, 2016, **1**, 16184.
- 7 Y. Yao, S. Hu, W. Chen, Z.-Q. Huang, W. Wei, T. Yao, R. Liu, K. Zang, X. Wang, G. Wu, W. Yuan, T. Yuan, B. Zhu, W. Liu, Z. Li, D. He, Z. Xue, Y. Wang, X. Zheng, J. Dong, C.-R. Chang, Y. Chen, X. Hong, J. Luo, S. Wei, W.-X. Li, P. Strasser, Y. Wu and Y. Li, *Nature Catalysis*, 2019, **2**, 304–313.
- 8 G. Kresse and J. Hafner, *Phys. Rev. B*, 1993, **47**, 558–561.
- 9 G. Kresse and J. Furthmüller, *Computational Materials Science*, 1996, **6**, 15–50.
- 10 G. Kresse and J. Furthmüller, *Phys. Rev. B*, 1996, **54**, 11169–11186.
- 11 J. P. Perdew, K. Burke and M. Ernzerhof, *Physical Review Letters*, 1996, **77**, 3865–3868.
- 12 H. J. Monkhorst and J. D. Pack, *Phys. Rev. B*, 1976, **13**, 5188–5192.